X-ray Fluorescence Spectroscopy and Imaging

BL6b: Micro-XRF

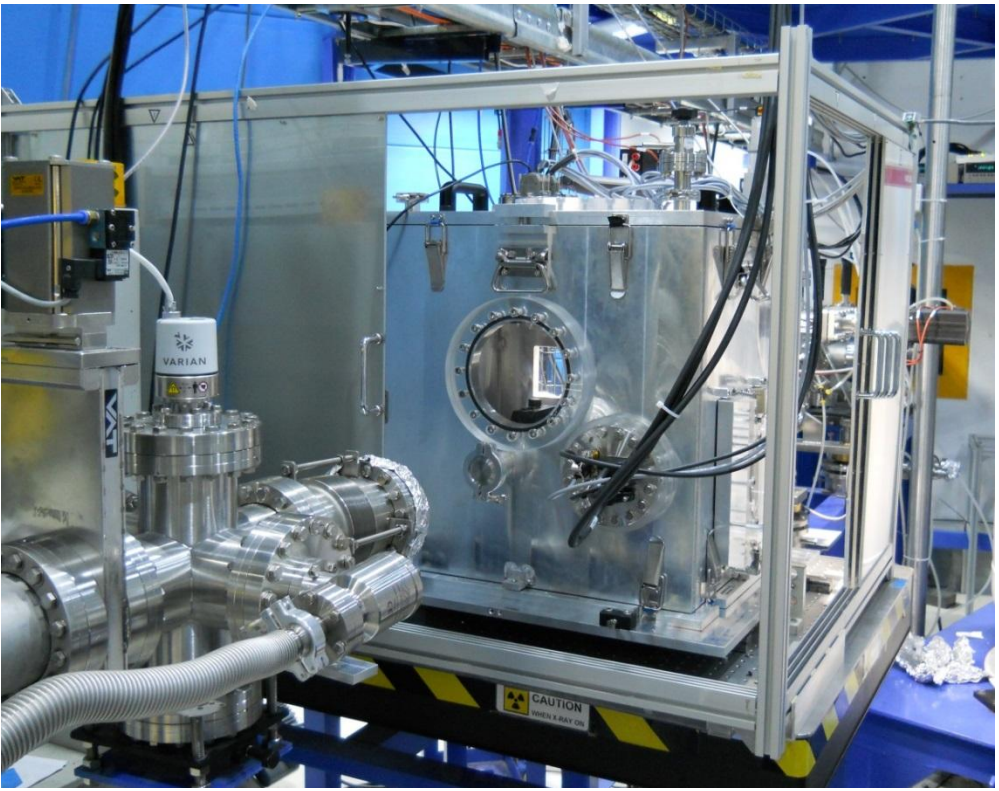

XRF Spectrometer

Scientists

Jitrin Chaiprapa, PhD
Nichada Jeeranaikun, PhD
Waraporn Tanthanuch, PhD

SYNCHROTRON THAILAND CENTRAL LAB

X-ray Fluorescence Spectroscopy and Imaging

XRF

Table 1 Chemical composition of marble sludge, wt.%.

Oxides	Content (%)
SiO_2	0.79
Al_2O_3	0.21
Fe_2O_3	0.06
CaO	55.42
MgO	0.25
SO_3^-	0.24
Na_2O	0.10
K_2O	0.02
P_2O_5	0.06
Cl^-	0.07
SrO	0.04
L.O.I	42.28
Total	99.54
Humidity	0.506
Water content	24.360

Key word: Chemical Compositions or Elemental Compositions

Micro-XRF

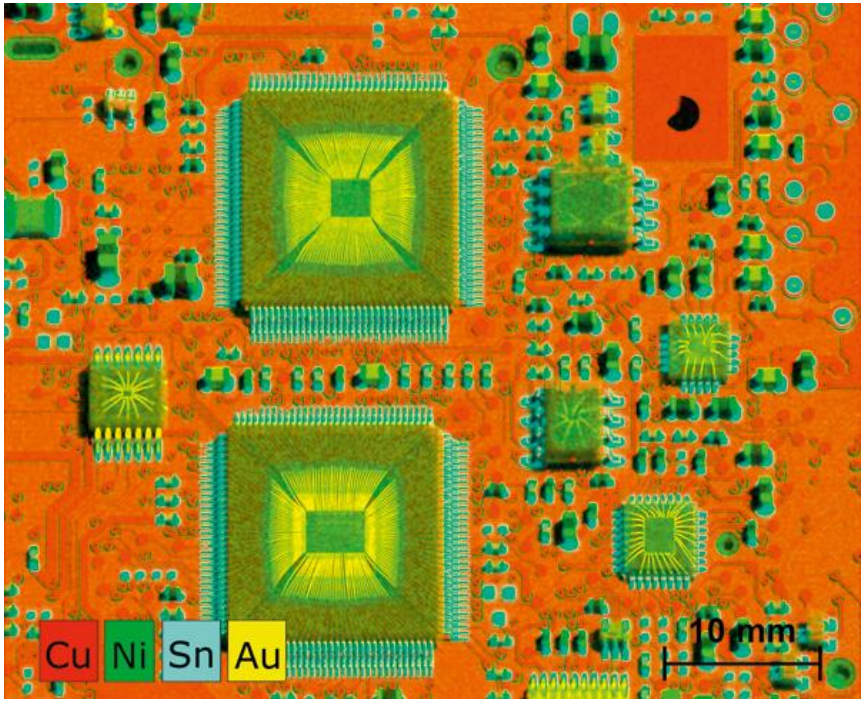

Key word: Elemental distributions

SYNCHROTRON THAILAND CENTRAL LAB

Manufacturing Processing Control

μXRF Investigations on the Influence of Solar Cell Processing Steps on Iron and Copper Precipitates in Multicrystalline Silicon

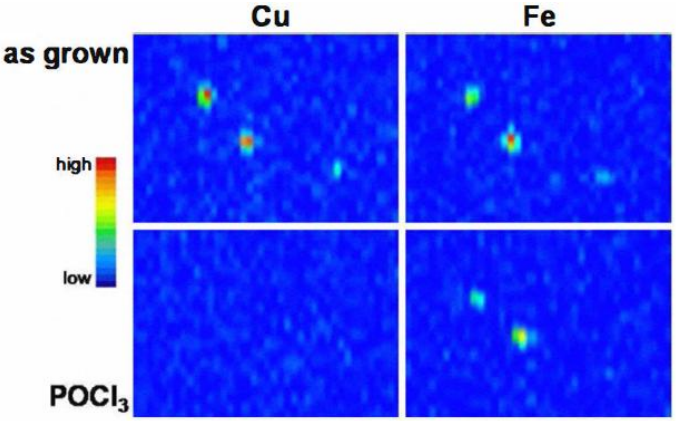

Fig. 1 μ-XRF mapping (3 x 2.1 μm) of Cu and Fe distribution before (top) and after (below) a phosphorous diffusion of $POCl_3$ [1].

[1] A. Zuschlag, Photovoltaic Specialists Conference (PVSC) IEEE, 2010, 000347-000351.

[2] M. Trushin et al., Nucl. Instr. Meth. Phys. Res. B, 2010, 268, 254–258.

XBIC/μXRF/μXAS analysis of metals precipitation in block-cast solar silicon

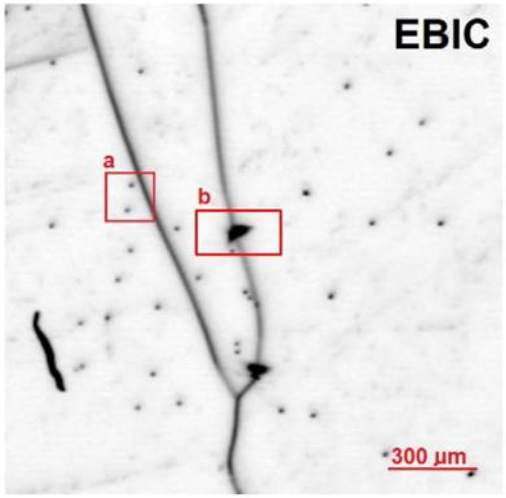

Fig. 2 Survey EBIC image and XRF maps of the defects in the Fe/Cu contaminated cast mc-Si sample [2].

(b)

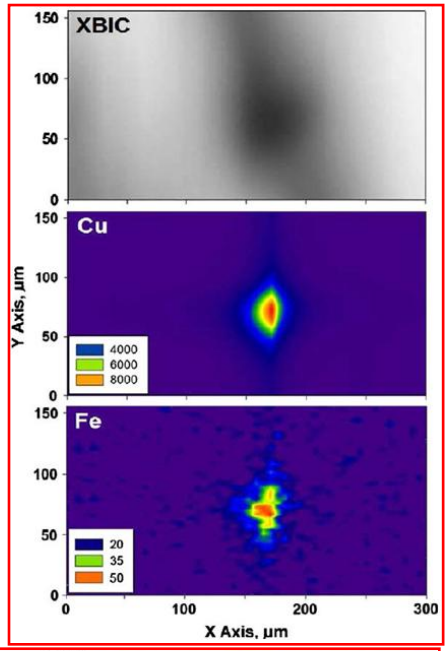

(a)

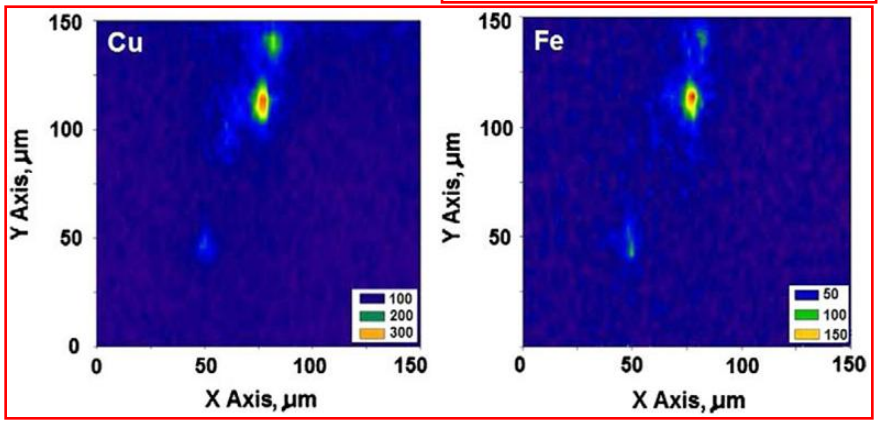

SYNCHROTRON THAILAND CENTRAL LAB

Manufacturing Processing Control

Continuous In-Line Processing of CdS/CdTe Devices: Process Control Using XRF and Efficient Heating

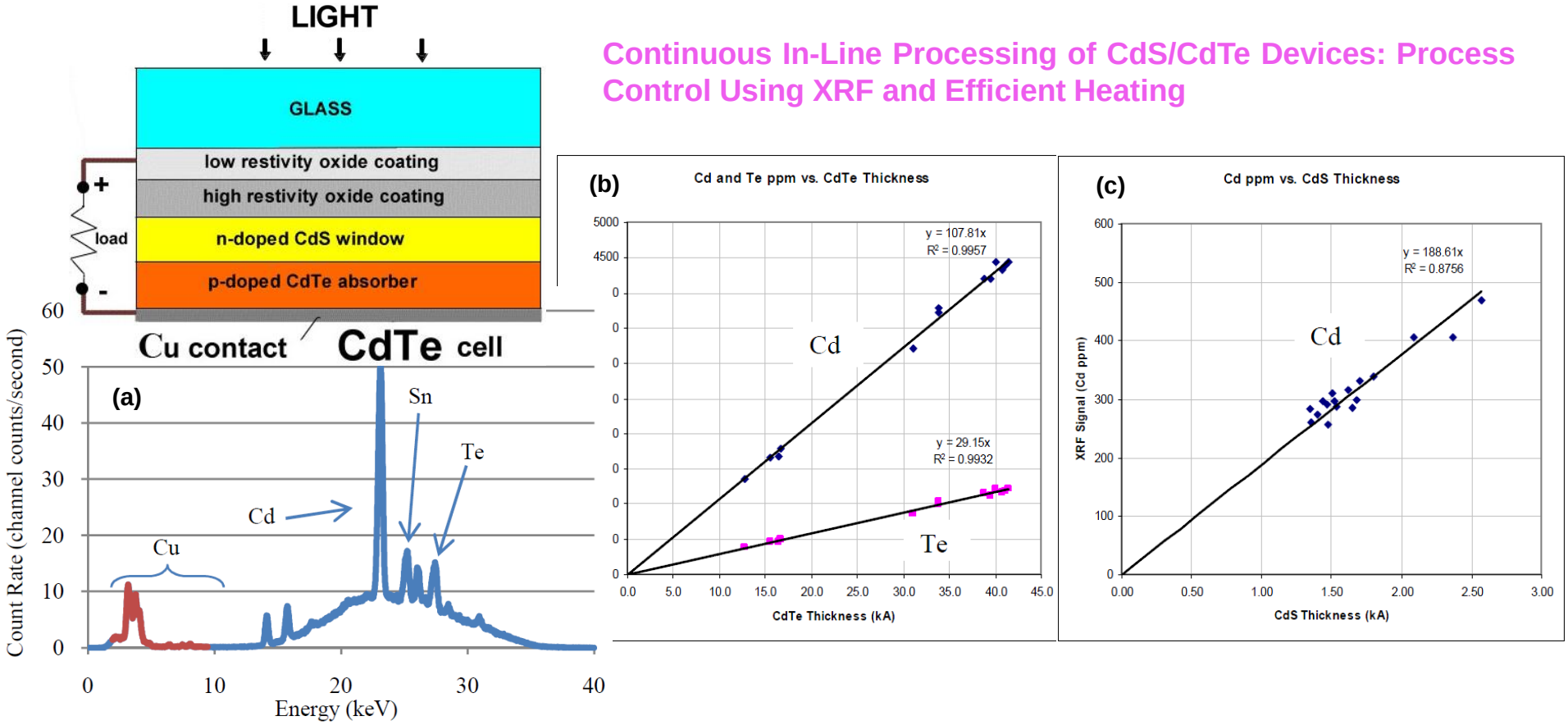

Fig. 3 (a) XRF spectrum of CdS/CdTe films on glass/TCO with Cu back contact. Film thickness correlations to XRF measured levels in (b) CdTe and (c) CdS films on glass/TCO using 5 minute measurement duration [3].

[3] P.S. Kobyakov, Photovoltaic Specialists Conference (PVSC) IEEE, 2010, 00780-00785.

SYNCHROTRON THAILAND CENTRAL LAB

Manufacturing Processing Control

Quality Assurance in PCB Manufacturing

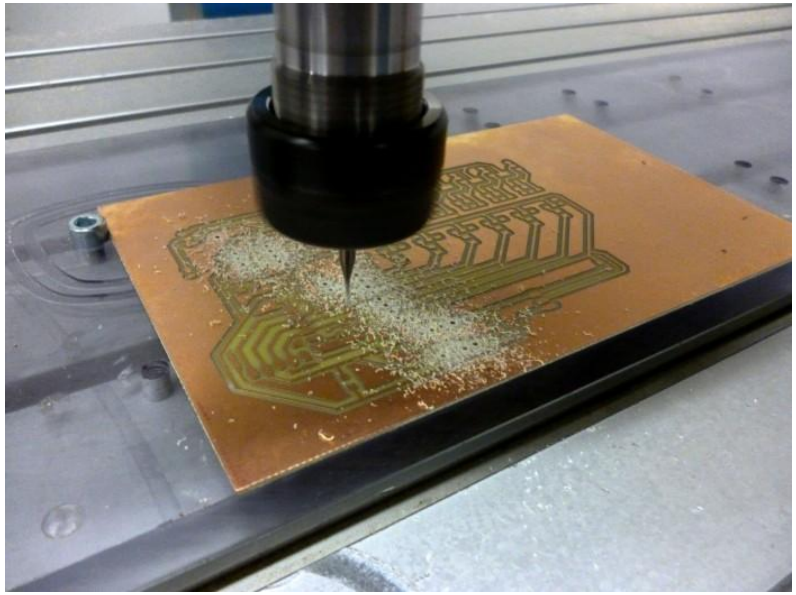

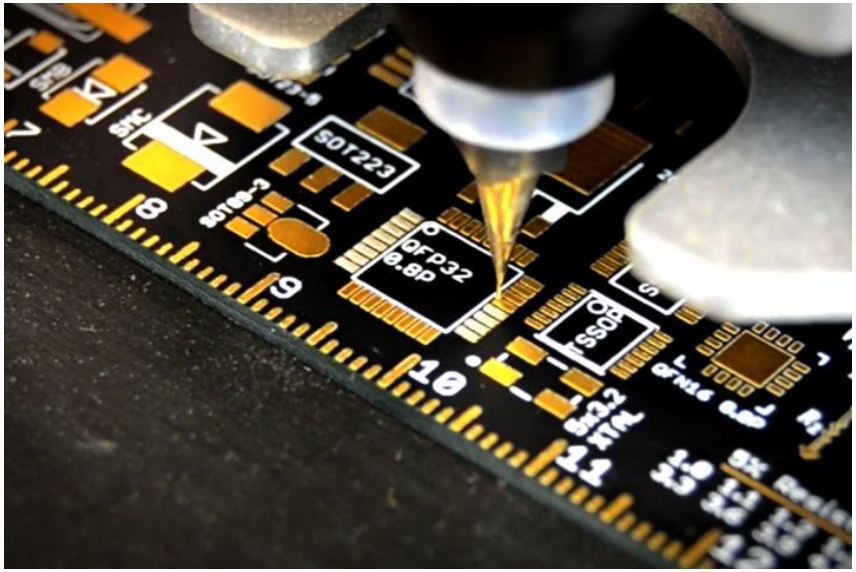

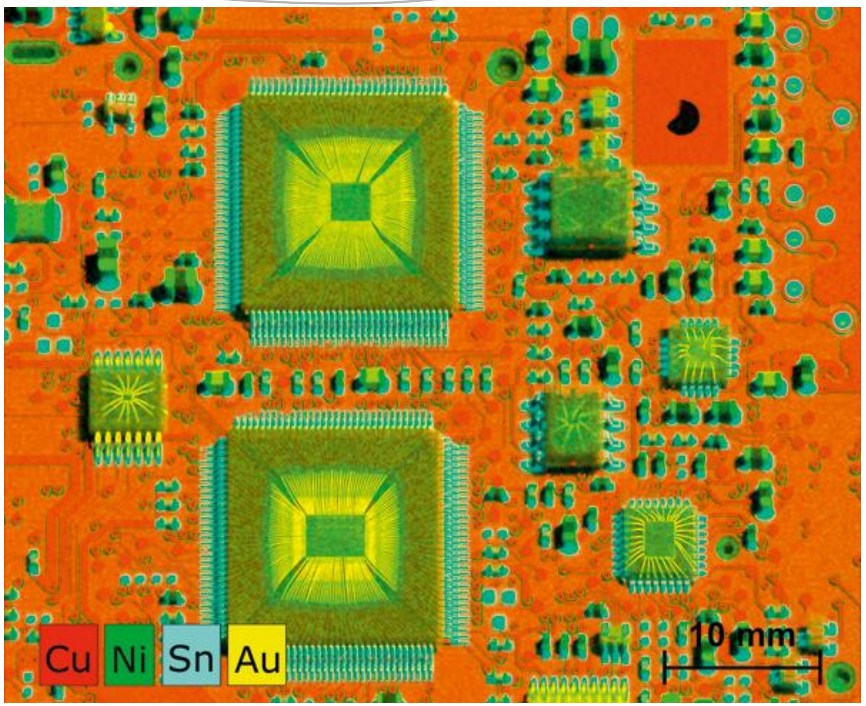

Elemental mapping of PCB

- ❖ **Gold Coatings in the nanometer range on PCBs**
- ❖ **Thickness Measurement of Conformal Coatings on PCBs**
- ❖ **Measuring the copper thickness in plated through-holes on PCBs**
- ❖ **Controlling the thickness of solder resist in the manufacture of PCBs**

SYNCHROTRON THAILAND CENTRAL LAB

Recycling Manufacturing Wastes

Characteristics of the marble processing powder waste At Shaq El-Thoaban industrial area, Egypt, and its suitability for cement manufacture

Table 1 Chemical composition of marble sludge, wt.%.

Oxides	Content (%)
SiO_2	0.79
Al_2O_3	0.21
Fe_2O_3	0.06
CaO	55.42
MgO	0.25
SO_3^-	0.24
Na_2O	0.10
K_2O	0.02
P_2O_5	0.06
Cl^-	0.07
SrO	0.04
L.O.I	42.28
Total	99.54
Humidity	0.506
Water content	24.360

SYNCHROTRON THAILAND CENTRAL LAB

[4] H.A. El-Sayed et al, Housing and Building National Research Center, ,2018, 14, 171-179.

Materials Characterization

Compositional analysis of Cementitious Materials

Micro-spectroscopic investigation of Al and S speciation in hardened cement paste

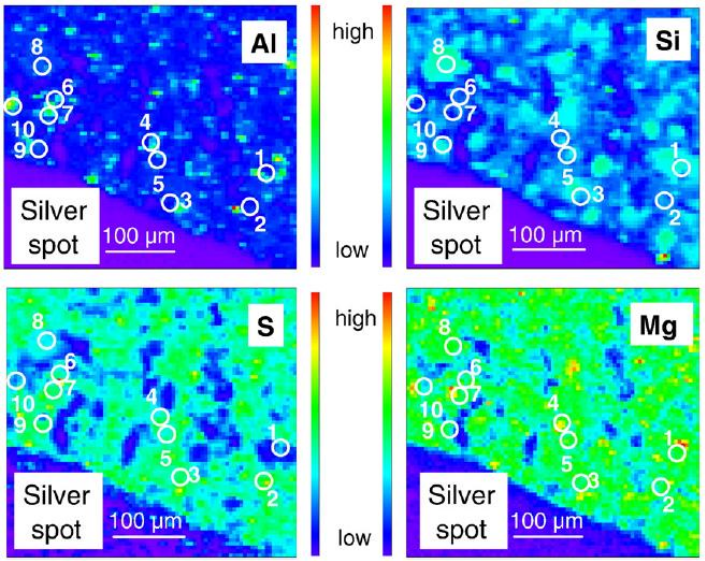

Fig. 4 Micro-XRF elemental distribution maps of Al, Si, S, and Mg in intact HCP hydrated at 50°C. Micro-XAS selected regions for S K-edge XANES measurements are marked with numbers. A silver spot was used as marker, which appears blue on the micro-XRF maps [5].

Determination of the elemental distribution and chemical speciation in highly heterogeneous cementitious materials using synchrotron-based micro-spectroscopic techniques

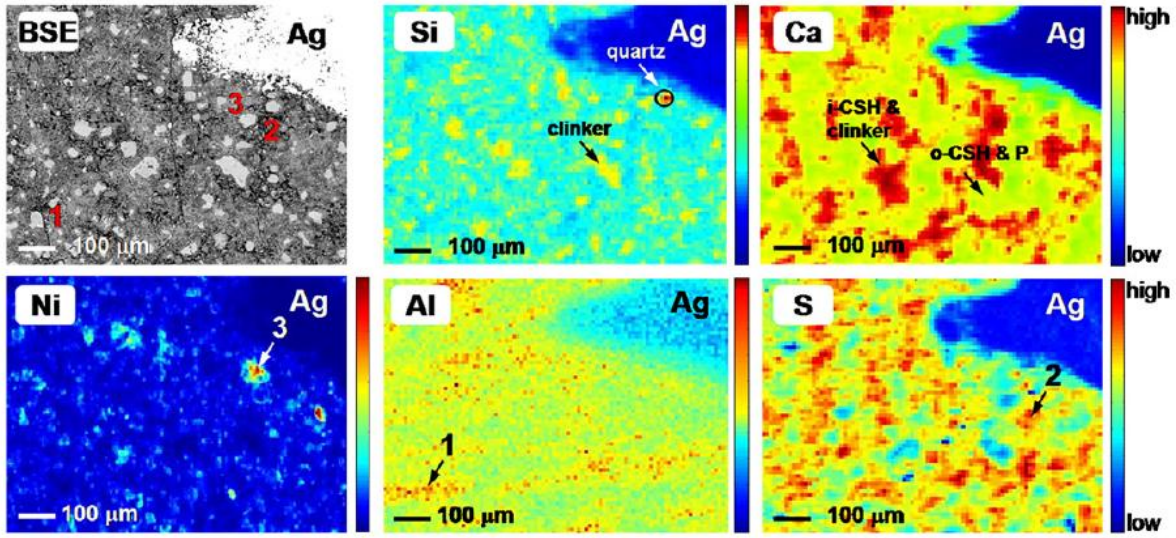

Fig. 5 BSE image and micro-XRF elemental distribution maps of Si, Ca, Ni, Al and S in a ~700×1000 µm overview of a Ni enriched hydrated cement matrix. Micro-XAS selected regions for Al K-edge (1), S K-edge (2) and Ni K-edge (3) measurements are marked with numbers on the BSE image and the respective elemental maps. Ag = silver spot used as marker [6].

[5] E. Wieland et al, Cement and Concrete Research, 2010, 40, 885–891.

[6] M. Vespa et al, Cement and Concrete Research, 2007, 37, 1473–1482.

SYNCHROTRON THAILAND CENTRAL LAB

Materials Characterization

Correlation between Chemical and Morphological Heterogeneities in $LiNi_{0.5}Mn_{1.5}O_4$ Spinel Composite Electrodes for Lithium-Ion Batteries Determined by Micro-X-ray Fluorescence Analysis

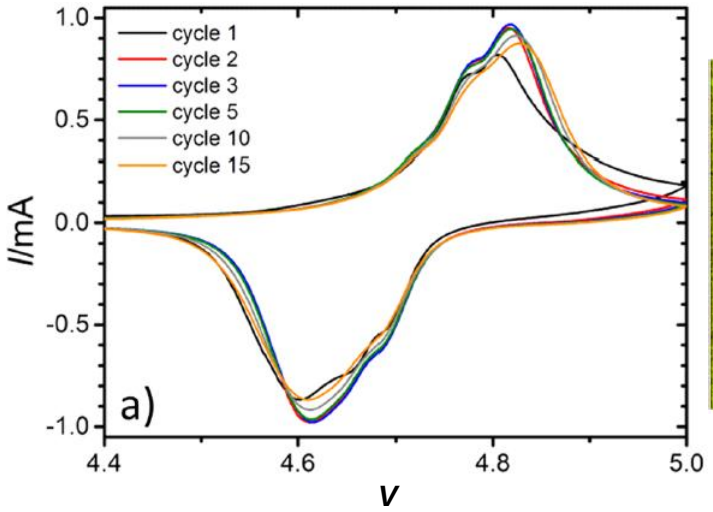

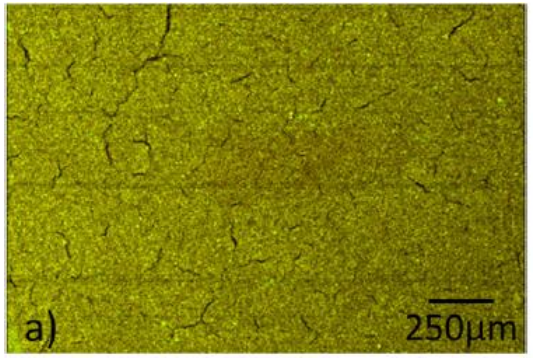

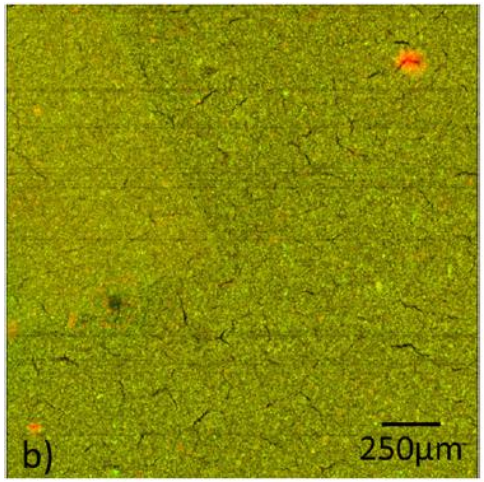

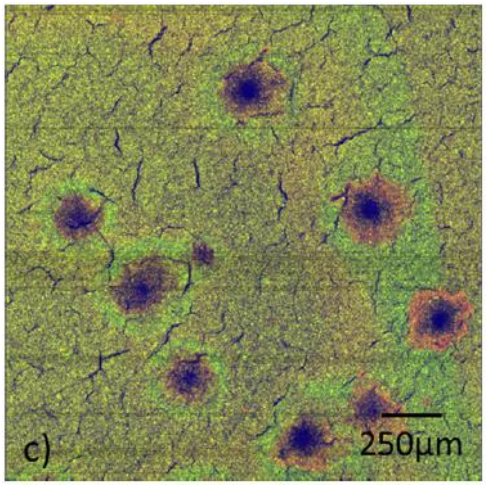

Figure 6 Electrodes cycled with (a) C/4, (b) C/2, and (c) 5 C for approximately 25 cycles. Green, Mn; red, Ni; and blue, transmission.

[7] U. Boesenberg et al, Chem. Mater., 2015, 27, 2525−2531.

SYNCHROTRON THAILAND CENTRAL LAB

Materials Characterization

In situ X-ray spectromicroscopy study of bipolar plate material stability for nano-fuel-cells with ionic-liquid electrolyte

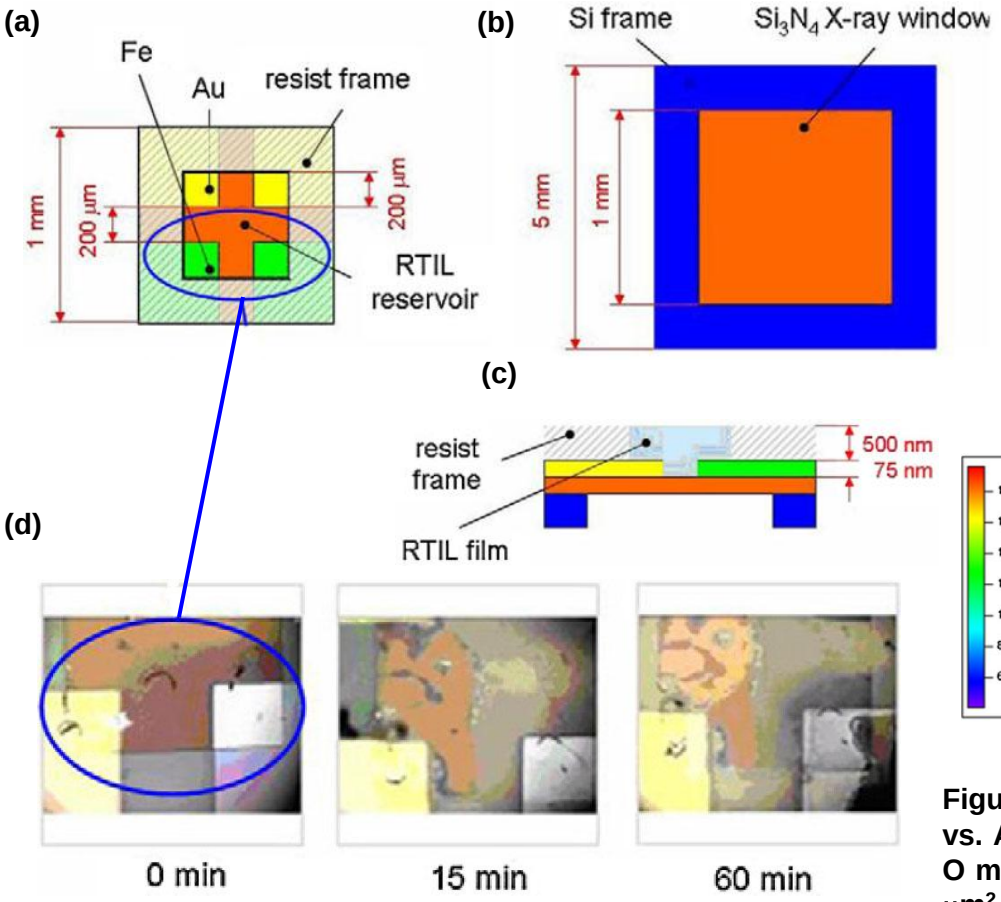

Figure 7a (a–c) Schematic view of the electrochemical cell, highlighting electrode and electrolyte layout (d) the optical micrograph of the electrochemical corrosion of the Fe electrodes.

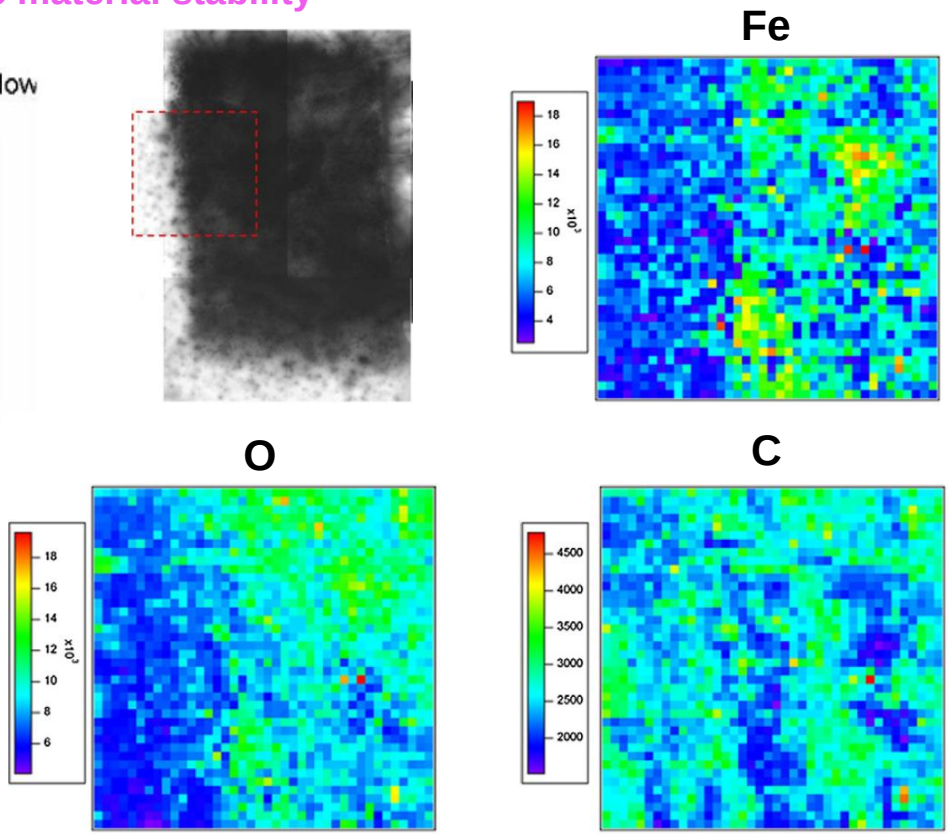

Figure 7b an STXM image of the Fe electrodes corroded at 200 mV vs. Au QRE for 1000 s (top left) and corresponding XRF C, Fe and O maps: the shown location in highlighted red square image 80x80 µm².

[8] B. Bozzini et al, Microelectronic Engineering, 2011, 88, 2456 2458.

SYNCHROTRON THAILAND CENTRAL LAB

Materials Characterization

Micro-XRF and micro-XAFS studies of an Al matrix Fe–Ni composite

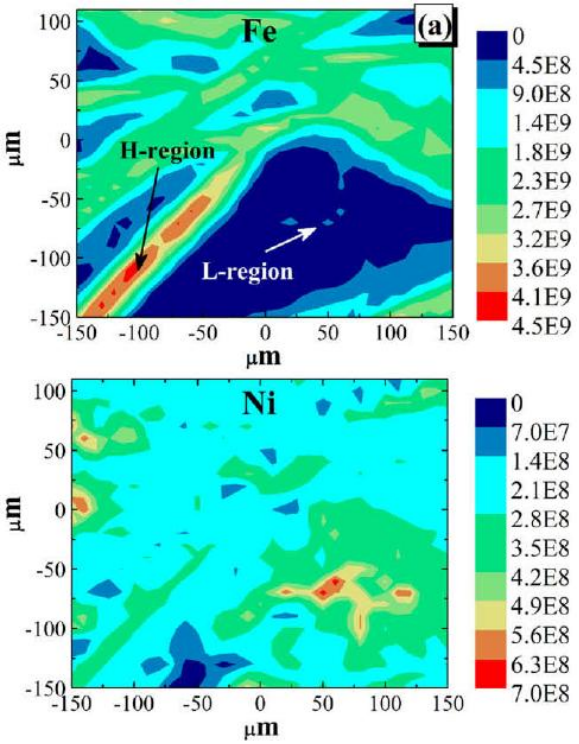

Fig. 8 300x260 μm² μ -XRF map of Al matrix Fe–Ni composite [9].

Synchrotron micro-XRF study of metal inclusions distribution and variation in fused silica induced by ultraviolet laser pulses

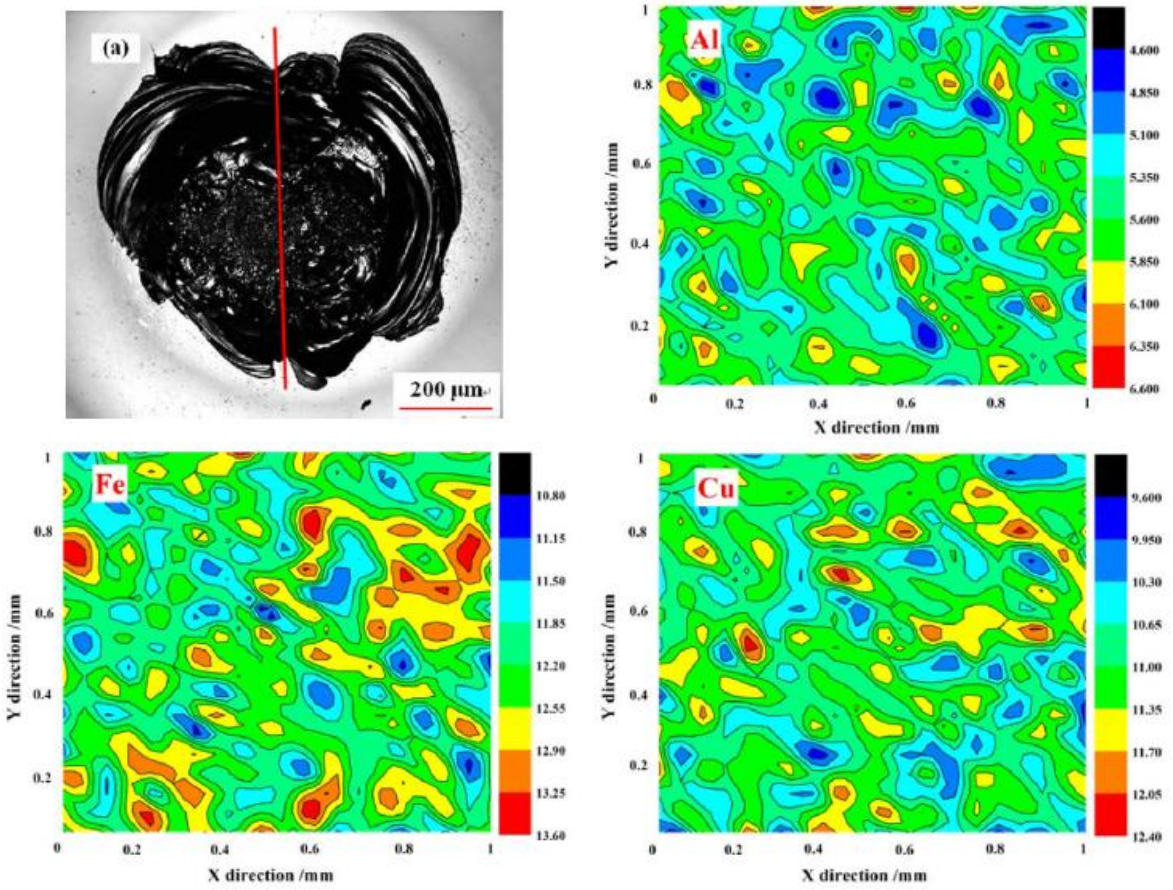

Fig. 9 Elemental maps of Al, Fe and Cu for the damage crater displayed in (a) [10].

[9] F. Pinakidou et al, Nuclear Instruments and Methods in Physics Research B, 2010, 268, 356–360.

[10] C.H. Li, Nuclear Instruments and Methods in Physics Research B, 2010, 268, 1502–1507.

SYNCHROTRON THAILAND CENTRAL LAB

Thank you
for your attention.

SYNCHROTRON
THAILAND
CENTRAL LAB